

Phase diagram of chiral quark matter: Fulde-Ferrell pairing from weak to strong coupling

Armen Sedrakian¹ and Dirk H. Rischke^{1,2}

¹*Institute for Theoretical Physics, J. W. Goethe University, D-60438 Frankfurt am Main, Germany*

²*Frankfurt Institute for Advanced Studies, D-60438 Frankfurt am Main, Germany*

(Dated: November 24, 2021)

We calculate the phase diagram of two-flavor quark matter in the temperature-flavor asymmetry plane in the case where there are three competing phases: the homogeneous Bardeen-Cooper-Schrieffer (BCS) phase, the unpaired phase, and a phase with broken spatial symmetry, which is here taken to be the counterpart of the Fulde-Ferrell (FF) phase in condensed matter physics. The system belongs to the universality class of paramagnetic-ferromagnetic-helical systems, and therefore contains a tricritical Lifshitz point in its phase diagram, where the momentum scale characterizing the breaking of translational invariance has a critical exponent of $1/2$ to leading order. We vary the coupling constant of the theory, which is obtained from integrating out the gluonic degrees of freedom. In weak coupling, the FF phase is favored at arbitrary flavor asymmetries for sufficiently low temperatures; at intermediate coupling its occupancy domain is shifted towards larger asymmetries. Strong coupling features a new regime of an inhomogeneous FF state, which we identify with a current-carrying Bose-Einstein condensate of tightly bound up and down quarks. The temperature and asymmetry dependence of the gap function is studied. It is shown that the anomalous temperature dependence of the gap in the homogeneous, flavor-asymmetric phase is transformed into a normal dependence (self-similar to the BCS phase) at arbitrary coupling, once the FF phase is allowed for. We analyze the occupation numbers and the Cooper-pair wave function and show that when the condensate momentum is orthogonal to the particle momentum the minority component contains a blocking region (breach) around the Fermi sphere in the weak-coupling limit, which engulfs more low-momentum modes as the coupling is increased, and eventually leads to a topological change in strong coupling, where the minority Fermi sphere contains either two occupied strips or an empty sphere. For non-orthogonal momenta, the blocking region is either reduced or extinct, i.e., no topological changes are observed.

PACS numbers: 12.38.Mh, 24.85.+p

I. INTRODUCTION

The phase diagram of dense hadronic matter is of great interest in relativistic astrophysics of compact stars and heavy-ion collisions. Because of the quark substructure of nucleons predicted by quantum chromodynamics (QCD), nuclear matter will undergo a phase transition to quark matter if squeezed to sufficiently high densities. In the quark matter phase the “liberated” quarks occupy continuum states which, in the low-temperature and high-density regime, arrange themselves in a Fermi sphere. In this regime quark matter will exhibit the phenomenon of pairing, or color superconductivity, because the quark-quark interaction is attractive in certain channels (early work on this subject is reviewed in Ref. [1]; various recent aspects are reviewed, e.g., in Refs. [2]).

Experimental verification of deconfined quark matter and color superconductivity can be found in the phenomenology of compact (neutron) stars [3, 4, 5, 6, 7, 8, 9, 10, 11]. The remnants of core-collapse supernovae is a hot and dense core of hadronic matter (the proto-neutron star), which rapidly cools from temperatures of the order of 100 MeV down to temperatures of the order of 1 MeV. The matter (in the baryonic or the deconfined quark matter phase) is initially nearly isospin symmetric. Electron capture on protons (u -quarks in deconfined quark matter) drives the isospin chemical poten-

tial up to values of the order of 100 MeV. Consequently, in parallel to rapid cooling, the isospin asymmetry of matter grows rapidly. In effect, compact stars traverse the temperature-isospin chemical potential plane from the high-temperature, low-isospin domain down to the low-temperature, high-isospin domain. One of the prime interests of this work is to compute the phase diagram of superconducting quark matter within this plane. The central problem is, of course, to predict the asymptotic state of matter reached during this evolution, since currently observable compact stars are in this asymptotic state, where they cool slowly from temperatures of the order of 100 keV down to 10 keV with nearly frozen composition [12, 13, 14, 15, 16].

The quark-quark interaction is strongest for pairing between up and down quarks which are antisymmetric in color [1, 2]. At intermediate densities quark matter is composed of up and down quarks, while strange quarks can appear in substantial amounts at higher densities. As the isospin chemical potential grows and reaches the asymptotic value determined by the β -equilibrium condition $\mu_d - \mu_u = \mu_e$ among d and u quarks and electrons, where μ_i with $i = d, u, e$ are the chemical potentials, the Fermi spheres of up and down quarks are shifted apart. The difference can reach values ~ 100 MeV, the magnitude of the electron chemical potential in β -equilibrated matter. Thus, the cross-flavor pairing must overcome the

disruptive effect of mismatched Fermi surfaces. Furthermore, if the physical strange quark mass is close to its current mass $M_s \sim 100$ MeV, electrons may be gradually replaced by strange quarks, which again will disfavor the cross-flavor pairing. Such a situation can be described by assuming that the densities (or alternatively the chemical potentials) of up and down quarks are unequal, as we shall do throughout this paper.

A superconducting phase with asymmetric cross-species pairing needs to optimize the overlap between the Fermi surfaces (which is perfect in the symmetric BCS state) to attain the maximum possible condensation energy. If temperature and correlations are negligible, an infinitesimal shift in the spherically symmetric, concentric Fermi surfaces is sufficient to destroy the superconducting phase. A less restrictive (and less symmetric) phase space configuration in which the condensate carries non-zero momentum with respect to some fixed frame is more flexible; the penalty in the energy budget for the (always positive) kinetic energy of condensate motion is compensated by the gain in the (negative) condensation energy. This class of phases was first studied by Fulde and Ferrell (FF) [17], who suggested a condensate order parameter that varies as $\Delta \sim \exp(i\mathbf{q} \cdot \mathbf{r})$, and by Larkin and Ovchinnikov (LO) [18], who explored a number of spatially varying parameters. The simple form of the FF order parameter permits to study this phase at arbitrary temperatures [19]. Larkin and Ovchinnikov used instead the Ginzburg-Landau theory, valid in the vicinity of a second-order phase transition, to analyze more complicated patterns of symmetry breaking (lattices). The quark matter counterparts of the FF phase have been discussed in Refs. [20, 21, 22, 23, 24, 25]. The quark matter counterparts of the Larkin-Ovchinnikov phase, within the Ginzburg-Landau approximation, have been studied in the two- and three-flavor cases in Refs. [26, 27, 28, 29, 30, 31]. In three-flavor quark matter the face-center cubic (fcc) lattices were identified as having particularly low free energy [28] in the regime where the Ginzburg-Landau (GL) theory is applicable. The spatial form of the condensate beyond the GL regime is not known. Furthermore, if the dynamics of the gluon field is retained, there appears the possibility of gluon condensation instead of the onset of macroscopic supercurrents [24, 32, 33, 34]. A more symmetric superconducting phase exploits deformations of Fermi spheres as the mechanism of restoring the coherence needed for pairing at the cost of kinetic energy loss caused by these deformations. The deformed Fermi surface phase requires minimal breaking of spatial symmetry and is more symmetric than the lattice phases above [35, 36, 37, 38]. To lowest order the deformations of the Fermi spheres break the rotational $O(3)$ symmetry down to $O(2)$. In this paper we shall adopt a particularly simple form of the order parameter: the single plane-wave FF ansatz. It shares many features with the more complex phases mentioned above and permits us to study the phases with broken spatial symmetry in a straightforward manner.

Our second key interest in this paper is to explore the phase diagram as the coupling is increased from its conventional value to larger values. To our knowledge this is the first investigation of asymmetric, *inhomogeneous* quark matter at strong coupling. As is well-known, for non-relativistic fermions the Nozieres-Schmitt-Rink [39] theory describes the mean-field evolution of the phase diagram from the BCS phase to the Bose-Einstein condensate (BEC) regime. This theory has been generalized to the case of unequal populations of fermions [40]. Furthermore, there are a number relativistic treatments of the problem for both matching and mismatched Fermi surfaces [41, 42, 43, 44, 45, 46, 47, 48]. Here we wish to extend the emerging picture of the phase diagram by including inhomogeneous, relativistic, phases of superconducting chiral fermions (quarks). While weak-coupling studies are likely to be sufficient for neutron star phenomenology, other superconducting systems may help to explore (experimentally) the strong-coupling regime as well. Examples are pairing in dilute alkali gases [49, 50, 51, 52, 53, 54, 55, 56, 57, 58], where density-imbalanced systems were created, for example, by using two hyperfine states of ${}^6\text{Li}$ fermionic isotopes, and graphene where the quasiparticle spectrum has relativistic form [59, 60, 61, 62].

Color superconductivity of quark matter can find its verification in the astrophysics of compact (neutron) stars and supernovae. The phase with broken spatial symmetry, such as the FF phase studied here or the crystalline phases with complex lattice structure, have their specific signatures which we shortly describe below. One avenue of discerning these phases in compact stars is through their cooling behavior [63, 64, 65, 66, 67, 68]. Normal quark matter cools too fast via the direct URCA process to account for measured neutron star surface temperatures. This implies that either quark stars are unobservable in the X-ray spectrum or quark matter is paired, the pairing gap preventing rapid cooling. Since the gaps are much larger than the relevant temperatures, pairing will effectively block the relevant neutrino processes. However, for the phases with broken spatial symmetry, not the entire Fermi surface is “gapped”; if this is so, cooling will take place at a reduced rate from the segments of the Fermi surface that are ungapped. In fact, it is possible to interpolate between the fully gapped and unpaired limits by assigning some amount of “gaplessness” in the spectrum of quasiparticles [64, 65, 66]. Another avenue is offered by the fact that crystalline color superconducting (CCS) matter may have shear moduli that are by orders of magnitude larger than those in neutron star crusts [69]. Consequently, CCS matter can support quadrupole deformations and can be a source of gravitational waves [70, 71, 72]. Upper limits on gravitational waves derived for known pulsars are within the range where the hypothesis of CCS matter in the cores of neutron stars can be tested [73].

Ab initio methods, such as lattice QCD, are (currently) not useful for studying the quark matter phase

diagram at high densities. Furthermore, in the density regime between twice and ten-fold nuclear saturation density, the coupling is too strong for perturbative QCD to be quantitatively accurate. Qualitative predictions are based either on the single-gluon exchange model or point-coupling effective models, such as the Nambu-Jona-Lasinio (NJL) model [2]. In this paper we shall start with the QCD Lagrangian, which contains explicit gluon fields and derive the Dyson-Schwinger equations describing the quark and gluon fields, and only at a later stage we will integrate them out. Such a methodology has been applied to homogeneous superconductors in Ref. [6]. Clearly, our final equations could have been also obtained directly from the NJL model Lagrangian without explicit reference to the QCD Lagrangian.

This paper is organized as follows. In Section II we set up the formalism to treat the FF and related phases in chiral quark matter. We start with the QCD partition function, perform a local transformation on the fields to allow for motion of pairs with non-zero momentum. The pairing fields are introduced via bosonization of the action after which we take the mean-field approximation. We write down the general Dyson-Schwinger equations for the quark and gluon propagators for our systems, after which the gluon propagator is postulated to have a contact form, which in turn eliminates the gluon fields and reduces the model to the four-fermion coupling NJL model. Our final equations (42)-(48) constitute four integral equations that must be solved simultaneously. Section III discusses the numerical results for the phase diagram, gap function, occupation numbers, and the kernel of the gap equation with attention to the differences between the strong- and weak-coupling regimes. In particular, we study the phase-space topological structure of the minority component in three interesting cases of weak, intermediate and strong coupling. We close with a discussion of our results in Section IV.

Appendix A shows the details of the transformation of the characteristic equation for the quasiparticle modes in the FF superconductor from the form that contain the propagators of the theory to a form that contains dispersion relations in the normal state and the gap function.

II. FORMALISM

The theory is described by the following functional integral

$$Z_{QCD} = \int \mathcal{D}\bar{\psi}\mathcal{D}\psi\mathcal{D}A_\mu^a \exp\left(\int d^4x\mathcal{L}_{QCD}\right), \quad (1)$$

where

$$\mathcal{L}_{QCD} = \bar{\psi}(i\gamma^\mu\partial_\mu - m)\psi - \frac{1}{4}(F_{\mu\nu}^a)^2 + g\bar{\psi}\gamma^\mu A_\mu\psi, \quad (2)$$

and ψ is the quark field, $A_\mu = A_\mu^a\lambda^a/2$ is the gluon field, λ_a are the Gell-Mann matrices, g is the strong coupling constant, m is the quark mass, $F_{\mu\nu}^a = \partial_\mu A_\nu^a - \partial_\nu A_\mu^a + gf^{abc}A_\mu^b A_\nu^c$ is the field strength tensor of the Yang-Mills field, f^{abc} are the structure constants. To eliminate gluons we write the generating functional (1)

$$Z_{QCD} = \int \mathcal{D}\bar{\psi}\mathcal{D}\psi \exp\left[\int d^4x\bar{\psi}(i\gamma^\mu\partial_\mu - m)\psi + \Gamma[j]\right], \quad (3)$$

where

$$\Gamma[j] = \log \int \mathcal{D}A \exp\left\{\int d^4x\left[-\frac{1}{4}(F_{\mu\nu}^a)^2 + gA_\mu^a j_\mu^a\right]\right\} \quad (4)$$

and $j_\mu^a = \bar{\psi}T^a\gamma^\mu\psi$ is the color current of quarks, $T_a = \lambda_a/2$ are the $SU(3)$ generators. Expanding the action (4) in powers of the quark current and keeping the leading order quadratic term we obtain [74]

$$\Gamma[j] = \frac{g^2}{2} \int d^4x d^4y j_\mu^a(x) D_{ab}^{\mu\nu}(x, y) j_\nu^b(y), \quad (5)$$

where $D_{\mu\nu}^{ab}(x, y)$ is the single-particle irreducible gluon correlation function in the pure Yang-Mills theory

$$D_{\mu\nu}^{ab}(x, y) = \langle A_\mu^a(x) A_\nu^b(y) \rangle - \langle A(x)_\mu^a \rangle \langle A_\nu^b(y) \rangle \quad (6)$$

and the brackets stand for average over the gluon field, i.e.,

$$\langle \dots \rangle = \frac{\int \mathcal{D}A \exp \dots \left(-\frac{1}{4} \int F^2\right)}{\int \mathcal{D}A \exp \left(-\frac{1}{4} \int F^2\right)}. \quad (7)$$

The partition function of the theory where the gluon field is integrated out is given by a path integral over the quark fields $\psi(x)$ as

$$\mathcal{Z} = \int \mathcal{D}\bar{\psi}\mathcal{D}\psi \exp\{S_0[\bar{\psi}, \psi] + S_I[\bar{\psi}, \psi]\}, \quad (8)$$

where the first term in the action is the free Fermi-gas contribution and the second term is the four-fermion gluon-mediated interaction contribution

$$S_0[\bar{\psi}, \psi] = \int d^4x d^4y \bar{\psi}(x) [G_0^+]^{-1}(x, y)\psi(y), \quad (9)$$

$$S_I[\bar{\psi}, \psi] = \frac{g^2}{2} \int d^4x d^4y \bar{\psi}(x) \Gamma_a^\mu \psi(x) D_{\mu\nu}^{ab}(x, y) \bar{\psi}(y) \Gamma_b^\nu \psi(y), \quad (10)$$

where $G_0^+(x, y)$ is the free quark propagator, $\Gamma_a^\mu = T_a \gamma^\mu$ is the quark-gluon vertex, and \pm superscripts on the quark propagator refer to fermions and charge-conjugate fermions. We consider hereafter the case of $N_f = 2$ flavors (u and d quarks) with $N_c = 3$ colors. Our basis is defined as

$$\psi = \begin{pmatrix} \psi_r^u \\ \psi_r^d \\ \psi_g^u \\ \psi_g^d \\ \psi_b^u \\ \psi_b^d \end{pmatrix}, \quad \bar{\psi} = (\bar{\psi}_r^u, \bar{\psi}_r^d, \bar{\psi}_g^u, \bar{\psi}_g^d, \bar{\psi}_b^u, \bar{\psi}_b^d). \quad (11)$$

Consider a local transformation on the quark fields given by

$$\psi' \rightarrow \psi e^{-i\theta(x)}, \quad \bar{\psi}' \rightarrow \bar{\psi} e^{i\theta(x)}. \quad (12)$$

We shall focus on the special case $\theta(x) = Q_\mu x^\mu / 2$, where the four vector $Q = (0, \mathbf{Q})$ has only a non-vanishing spatial component. The transformation (12) breaks the translational symmetry of the theory. The particular form of the transformation leads to the free quark propagator with non-vanishing momentum $\mathbf{Q}/2$ with respect to some fixed frame. Under the transformation (12) the kinetic part of the partition function retains its form, however the free quark Green's function becomes (flavor and color indices are suppressed)

$$[\tilde{G}_0^+]^{-1}(x, y) = [G_0^+]^{-1}(x, y) + [\gamma^\mu \partial_\mu \theta(y)] \delta(x - y). \quad (13)$$

The effect of the transformation becomes transparent if we examine the Fourier transform of the propagator (13)

$$[\tilde{G}_0^\pm]^{-1} = \gamma^\mu (\pm Q_\mu / 2 + k_\mu) \pm \mu \gamma_0 - m, \quad (14)$$

which is seen to be identical to the Fourier transform of the propagator $[G_0^\pm]^{-1}$ with respect to the relative and center-of-mass space-time coordinates in a frame with non-vanishing center-of-mass momentum \mathbf{Q} . Here μ is the chemical potential associated with the conserved baryon charge. The action is bosonized by introducing pair fields

$$\Xi^+(x, y) = g^2 \bar{\Gamma}_a^\mu \langle \psi_C(x) \bar{\psi}(y) \rangle \Gamma_b^\nu D_{\mu\nu}^{ab}(x, y), \quad \Xi^-(y, x) = \gamma_0 [\Delta^+(x, y)]^\dagger \gamma_0, \quad (15)$$

where $\bar{\Gamma}_a^\mu = C(\Gamma_a^\mu)^T C^{-1} = -T_a^T \gamma^\mu$. The interaction term of the action will be evaluated in the mean-field approximation by keeping the leading-order term in the expansion with respect to the deviations of the two-point function $K(x, y) = \psi_C(x) \bar{\psi}(y)$ from its mean value $\langle K(x, y) \rangle$. In this approximation the partition function is given by

$$\begin{aligned} \mathcal{Z}_{\text{MF}} &= \int \mathcal{D}\psi \mathcal{D}\bar{\psi} \exp \{ S_\Xi[\bar{\psi}, \psi] \} \\ &\times \exp \left\{ \frac{g^2}{4} \int dx dy \text{Tr} [\gamma_0 \langle K^\dagger(y, x) \rangle \gamma_0 \bar{\Gamma}_a^\mu \langle K(x, y) \rangle \Gamma_b^\nu + \langle K(x, y) \rangle \Gamma_b^\nu \gamma_0 \langle K^\dagger(y, x) \rangle \gamma_0 \bar{\Gamma}_a^\mu] D_{\mu\nu}^{ab}(x, y) \right\}, \quad (16) \end{aligned}$$

where the trace is over Dirac, color, and flavor indices and

$$S_\Xi[\psi, \bar{\psi}] = \int dx dy \left\{ \bar{\psi}(x) [\tilde{G}_0^+]^{-1}(x, y) \psi(y) + \frac{1}{2} [\bar{\psi}_C(x) \Xi^+(x, y) \psi(y) + \bar{\psi}(y) \Xi^-(y, x) \psi_C(x)] \right\}. \quad (17)$$

We now rewrite the functional integral in terms of Nambu-Gorkov spinor fields

$$\Psi = \begin{pmatrix} \psi \\ \psi_C \end{pmatrix}, \quad \bar{\Psi} = (\bar{\psi}, \bar{\psi}_C), \quad (18)$$

where $\psi_C = C \bar{\psi}^T$ is the charge-conjugate spinor; C is the charge-conjugation matrix. In this basis, the full propagator and the self-energy are given by

$$\mathcal{G} = \begin{pmatrix} \tilde{G}^+ & F^- \\ F^+ & \tilde{G}^- \end{pmatrix}, \quad \Omega = \begin{pmatrix} \Sigma^+ & \Xi^- \\ \Xi^+ & \Sigma^- \end{pmatrix}. \quad (19)$$

Their elements are related by the Schwinger-Dyson equations

$$[\tilde{G}^\pm]^{-1} = [\tilde{G}_0^\pm]^{-1} + \Sigma^\pm - \Xi^\mp \left([\tilde{G}_0^\mp]^{-1} + \Sigma^\mp \right)^{-1} \Xi^\pm, \quad (20)$$

$$F^\pm = - \left([\tilde{G}_0^\mp]^{-1} + \Sigma^\mp \right)^{-1} \Xi^\pm \tilde{G}^\pm, \quad (21)$$

where F^\pm is the so-called anomalous propagator. We will ignore the normal self-energy Σ^\pm in the following. At the mean-field level the partition function is then given by

$$\mathcal{Z}_{\text{MF}} = [\det_k(\beta\mathcal{G}^{-1})]^{1/2} \exp \left\{ \frac{g^2}{2\beta} \int \frac{d^4k}{(2\pi)^4} \int \frac{d^4p}{(2\pi)^4} \text{Tr} [F^-(k) \bar{\Gamma}_a^\mu F^+(p) \Gamma_b^\nu] D_{\mu\nu}^{ab}(k-p) \right\}, \quad (22)$$

where β is the inverse temperature, $d^4k \equiv dk_0 d^3k$, where the k_0 integration is understood as summation over the discrete fermionic Matsubara frequencies; note that the trace runs over color, Dirac, flavor spaces; the trace over the Nambu-Gorkov space has been carried out.

In the following we shall restrict our discussion to the chiral limit of massless quarks. In this case the free quark propagator is diagonal in color and flavor space

$$\tilde{G}_0^\pm = \text{diag} \left(\tilde{G}_0^{\pm u}, \tilde{G}_0^{\pm d}, \tilde{G}_0^{\pm u}, \tilde{G}_0^{\pm d}, \tilde{G}_0^{\pm u}, \tilde{G}_0^{\pm d} \right). \quad (23)$$

The gap functions, in the basis (11), are given by

$$\Xi^\pm = \begin{pmatrix} 0 & 0 & 0 & \Xi_1^\pm & 0 & 0 \\ 0 & 0 & \Xi_2^\pm & 0 & 0 & 0 \\ 0 & \Xi_2^\pm & 0 & 0 & 0 & 0 \\ \Xi_1^\pm & 0 & 0 & 0 & 0 & 0 \\ 0 & 0 & 0 & 0 & 0 & 0 \\ 0 & 0 & 0 & 0 & 0 & 0 \end{pmatrix}. \quad (24)$$

We shall expand the gap matrices in the basis of positive and negative states

$$\Xi_{1,2}^\pm(k) = \sum_e \Delta_{1,2}^e(k) \Lambda^e(\mathbf{k}), \quad (25)$$

where $\Lambda^e(\mathbf{k}) = (1 + e\gamma_0 \boldsymbol{\gamma} \cdot \mathbf{k}/|\mathbf{k}|)/2$ are the projectors onto the positive $e = +$ and negative $e = -$ energy states in the chiral limit.

The full \tilde{G}^\pm propagator is diagonal in color-flavor space and its elements can be read off from the Schwinger-Dyson Eq. (20). The full anomalous propagator has a matrix form identical to Eq. (24)

$$F^\pm = \begin{pmatrix} 0 & 0 & 0 & F_{rg}^{\pm ud} & 0 & 0 \\ 0 & 0 & F_{rg}^{\pm du} & 0 & 0 & 0 \\ 0 & F_{gr}^{\pm ud} & 0 & 0 & 0 & 0 \\ F_{gr}^{\pm du} & 0 & 0 & 0 & 0 & 0 \\ 0 & 0 & 0 & 0 & 0 & 0 \\ 0 & 0 & 0 & 0 & 0 & 0 \end{pmatrix}, \quad (26)$$

with the elements that follow from the Schwinger-Dyson equation (21)

$$F_{rg}^{\pm ud} = -\tilde{G}_{0r}^{\mp u} \Xi_1^\pm \tilde{G}_g^{\pm d}, \quad F_{rg}^{\pm du} = -G_{0r}^{\mp d} \Xi_2^\pm \tilde{G}_g^{\pm u}, \quad (27)$$

$$F_{gr}^{\pm ud} = -G_{0g}^{\mp u} \Xi_2^\pm \tilde{G}_r^{\pm d}, \quad F_{gr}^{\pm du} = -G_{0g}^{\mp d} \Xi_1^\pm \tilde{G}_r^{\pm u}. \quad (28)$$

The quasiparticle excitation spectrum is given by the eigenvalues of the fermionic determinant in Eq. (22). Equivalently, it is given by the poles of the propagators in Eqs. (20) and (21), i.e., by $[\tilde{G}^\pm]^{-1} = [F^\pm]^{-1} = 0$. For the paired quarks this translates into the characteristic equation for the modes

$$\left(\tilde{G}_{0i}^{-f} \right)^{-1} \left(\tilde{G}_{0j}^{+g} \right)^{-1} - \sum_e |\Delta_{ij}^{efg}|^2 \Lambda^e(\mathbf{k}) = 0, \quad (29)$$

where the indices i, j and f, g label the (admissible combinations of) color and flavor indices, respectively. The solution to Eq. (29) reads (see Appendix A for details)

$$E_e^\pm(\Delta_{1,2}^e) = E_{A,e} \pm \sqrt{E_{S,e}^2 + |\Delta_{1,2}^e|^2}, \quad (30)$$

where $E_{S,e}$ and $E_{A,e}$ are the parts of the spectrum which are even (symmetric) and odd (asymmetric) under exchange of quark flavors in a Cooper pair. These are given by

$$E_{S,e}(|\mathbf{k}|, |\mathbf{Q}|, \theta, \bar{\mu})^2 = (|\mathbf{k}| - e\bar{\mu})^2, \quad (31)$$

$$E_{A,e}(|\mathbf{Q}|, \theta, \delta\mu) = \delta\mu + e|\mathbf{Q}|\cos\theta, \quad (32)$$

where θ is the angle formed by vectors \mathbf{k} and \mathbf{Q} , $\delta\mu = (\mu_i - \mu_j)/2$ and $\bar{\mu} = (\mu_i + \mu_j)/2$. The spectrum of unpaired blue quarks can be obtained as above by neglecting the contribution from the anomalous self-energy to the propagator. We quote only the final result, which is given by $\xi_e^\pm(\mathbf{k}, \mu_b) = E_{S,e}^\pm(\mathbf{k}, 0, 0, \mu_b)$, where μ_b is the chemical potential of blue quarks.

In the following we reduce our model to the NJL model featuring a contact four-fermion interaction. The momentum-space gluon propagator for a contact interaction has the simple form

$$D_{\mu\nu}^{ab} = \delta^{ab} \frac{g_{\mu\nu}}{\Lambda^2}, \quad (33)$$

where Λ is a characteristic momentum scale. Upon inserting this result into Eq. (22), evaluating the fermionic determinant, and carrying out the summation over the Matsubara frequencies we find

$$\ln \mathcal{Z}_{\text{MF}} = \ln \mathcal{Z}_{\text{MF}}^\Delta + \ln \mathcal{Z}_{\text{MF}}^0, \quad (34)$$

where the first term includes the contribution from the condensate of red-green quarks and the second term is the contribution from the non-interacting blue quarks. The first term is given by

$$\begin{aligned} \ln \mathcal{Z}_{\text{MF}}^\Delta &= \frac{3}{8} \frac{\Lambda^2}{g^2} \beta \sum_n (|\Delta_n^+|^2 + 3 \sum_{n', n \neq n'} \Delta_n^+ \Delta_{n'}^+) \\ &+ \frac{1}{2} \sum_{e,n} \int \frac{d^3k}{(2\pi)^3} \left\{ \beta [E_e^+(\Delta_n^e) - E_e^-(\Delta_n^e)] - 2 \ln f[-E_e^+(\Delta_n^e)] - 2 \ln f[-E_e^-(\Delta_n^e)] \right\}, \end{aligned} \quad (35)$$

where $f(\omega) = [1 + \exp(\beta\omega)]^{-1}$ is the Fermi distribution. The contribution of the blue quarks is

$$\ln \mathcal{Z}_{\text{MF}}^0 = 2 \int \frac{d^3k}{(2\pi)^3} \sum_{e,f} \left\{ -\ln f[-\xi_e^+(\mathbf{k}, \mu_{b,f})] - \ln f[-\xi_e^-(\mathbf{k}, \mu_{b,f})] \right\}. \quad (36)$$

The thermodynamic potential is obtained from the logarithm of the partition function as

$$\Omega_{\text{MF}} = -\frac{1}{\beta} \ln \mathcal{Z}_{\text{MF}}. \quad (37)$$

The stationary point(s) of the thermodynamic potential determine the equilibrium values of the order parameters

$$\frac{\partial \Omega_{\text{MF}}}{\partial \Delta_1^e} = 0, \quad \frac{\partial \Omega_{\text{MF}}}{\partial \Delta_2^e} = 0, \quad \frac{\partial \Omega_{\text{MF}}}{\partial |\mathbf{Q}|} = 0. \quad (38)$$

The direction of the vector \mathbf{Q} is chosen by the superconductor spontaneously. We shall work at fixed baryonic density and nonzero temperature. We shall consider variations in the relative concentrations of the u and d quarks, which are determined from the derivative of the thermodynamic potential with respect to the corresponding chemical potential as

$$\frac{\partial \Omega_{\text{MF}}}{\partial \mu_u} = n_u, \quad \frac{\partial \Omega_{\text{MF}}}{\partial \mu_d} = n_d. \quad (39)$$

The explicit form of the gap equations follows upon minimization as

$$\Delta_1 + 3\Delta_2 = -\frac{2g^2}{3\Lambda^2} \sum_e \int \frac{d^3p}{(2\pi)^3} \frac{2\Delta_1^e}{E_e^+(\Delta_1^e) - E_e^-(\Delta_1^e)} \left\{ \tanh \left[\frac{\beta}{2} E_e^+(\Delta_1^e) \right] + \tanh \left[\frac{\beta}{2} E_e^-(\Delta_1^e) \right] \right\}, \quad (40)$$

$$3\Delta_1 + \Delta_2 = -\frac{2g^2}{3\Lambda^2} \sum_e \int \frac{d^3p}{(2\pi)^3} \frac{2\Delta_2^e}{E_e^+(\Delta_2^e) - E_e^-(\Delta_2^e)} \left\{ \tanh \left[\frac{\beta}{2} E_e^+(\Delta_2^e) \right] + \tanh \left[\frac{\beta}{2} E_e^-(\Delta_2^e) \right] \right\}. \quad (41)$$

Note that the minima are degenerate with respect to the particle charge index e , consequently we have dropped this index on the left-hand sides of the gap equations. Because the kernels on the right-hand side of the two gap equations are invariant under the interchange $1 \leftrightarrow 2$ the two gap functions must be degenerate $\Delta_1 = -\Delta_2 = \Delta$, i.e. we are left with a single gap equation

$$\Delta = -\frac{2g^2}{3\Lambda^2} \sum_e \int \frac{d^3p}{(2\pi)^3} \frac{\Delta}{E_e^+(\Delta^e) - E_e^-(\Delta^e)} \left\{ \tanh \left[\frac{\beta}{2} E_e^+(\Delta^e) \right] + \tanh \left[\frac{\beta}{2} E_e^-(\Delta^e) \right] \right\}. \quad (42)$$

In the symmetric limit $E_e^+(\Delta^e) = E_e^-(\Delta^e)$ and when $|\mathbf{Q}| = 0$ the gap equation reduces to the ordinary BCS gap equation for ultrarelativistic fermions. The densities of paired up and down quarks are given by

$$n_d - \frac{n_b}{2} = -\frac{1}{2} \sum_{e,n} \int \frac{d^3k}{(2\pi)^3} \left\{ \frac{\partial E_e^+(\Delta_n^e)}{\partial \mu_d} \tanh \left[\frac{\beta}{2} E_e^+(\Delta_n^e) \right] - \frac{\partial E_e^-(\Delta_n^e)}{\partial \mu_d} \tanh \left[\frac{\beta}{2} E_e^-(\Delta_n^e) \right] \right\}, \quad (43)$$

$$n_u - \frac{n_b}{2} = -\frac{1}{2} \sum_{e,n} \int \frac{d^3k}{(2\pi)^3} \left\{ \frac{\partial E_e^+(\Delta_n^e)}{\partial \mu_u} \tanh \left[\frac{\beta}{2} E_e^+(\Delta_n^e) \right] - \frac{\partial E_e^-(\Delta_n^e)}{\partial \mu_u} \tanh \left[\frac{\beta}{2} E_e^-(\Delta_n^e) \right] \right\}, \quad (44)$$

where n_b is the number density of blue quarks and

$$\frac{\partial E_e^\pm(\Delta_{1,2}^e)}{\partial \mu_d} = \frac{1}{2} \left(1 \mp \frac{eE_{S,e}}{\sqrt{E_{S,e}^2 + |\Delta_{1,2}^e|^2}} \right), \quad (45)$$

and

$$\frac{\partial E_e^\pm(\Delta_{1,2}^e)}{\partial \mu_u} = -\frac{1}{2} \left(1 \pm \frac{eE_{S,e}}{\sqrt{E_{S,e}^2 + |\Delta_{1,2}^e|^2}} \right). \quad (46)$$

The contribution of the unpaired quarks to the density is given by

$$n_b = 2 \int \frac{d^3k}{(2\pi)^3} \sum_{e,f} \left\{ f[\xi_e^+(\mathbf{k}, \mu_{b,f})] - f[\xi_e^-(\mathbf{k}, \mu_{b,f})] \right\}. \quad (47)$$

The total quark density is $n_u + n_d + n_b = 3n_B$, where n_B is the baryonic density. Finally, the equation for total momentum is given by

$$0 = -\sum_{ee'} \int \frac{d^3k}{(2\pi)^3} \left(ee' \cos \theta + \frac{E_{S,e}}{\sqrt{E_{S,e}^2 + |\Delta^e|^2}} \frac{\partial E_{S,e}}{\partial |\mathbf{Q}|} \right) \tanh \left[\frac{1}{2} E_e^e(\Delta^e) \right]. \quad (48)$$

The zero temperature counterparts of the Eqs. (42)-(48) are straightforward to obtain with the help of the identity $\tanh(x/2) = 1 - 2f(x)$ and the limiting form of the Fermi distribution function $f(x) = \theta(-x)$ as $\beta \rightarrow \infty$, where $\theta(x)$ is the Heaviside step function.

Massive strange quarks can be present in matter, but may not participate in the pairing with the u and d quarks. This requires the strange quark mass to be larger than the chemical potential mismatch, since otherwise the cross flavor pairing with strange quarks can not be ignored (in other words, we ignore the possibility of the color-flavor-locking type pairing). Under such circumstances the contribution of strange quarks to the thermodynamical potential is straightforward to write down

$$\Omega_s = \frac{2}{\beta} \int \frac{d^3k}{(2\pi)^3} \sum_{e,c} \left\{ \ln f[-E_{s,e}^+(\mathbf{k}, \mu_{c,s})] + \ln f[-E_{s,e}^-(\mathbf{k}, \mu_{c,s})] \right\}, \quad (49)$$

where $E_{s,e}^\pm = \sqrt{k^2 + m_s^2}$. Here, m_s is the strange quark mass, which is expected to lie within the range $100 \leq m_s \leq 500$ MeV.

III. RESULTS

the four integral equations for the gap, the densities of up

The model defined by Eqs. (42)-(48) was solved numerically by finding a solution that satisfies simultaneously

and down quarks, and the nonzero momentum of the condensate. The ultraviolet divergence of the integrals was regularized by a three-dimensional cut-off in momentum space $|\mathbf{p}| < \Lambda_{NJL}$. The phenomenological value of the coupling constant $G = g^2/12\Lambda^2$ in the $\langle qq \rangle$ Cooper channel is related to the coupling constant in the $\langle \bar{q}q \rangle$ di-quark G_d channel by the relation $G = N_c/(2N_c - 2)G_d$, where $N_c = 3$ is the number of quark colors. The coupling constant G_d and the cut-off Λ_{NJL} are fixed by adjusting the model to the vacuum mass and decay constant of the pion. We employ the parameter set $G_d = 3.11 \text{ GeV}^{-2}$ and $G_d\Lambda_{NJL}^2 = 1.31$.

Our discussion below will be carried out at fixed baryonic density $n_B = 0.55 \text{ fm}^{-3}$. We wish to explore the behavior of our model under variations of temperature, density asymmetry (or, equivalently, the asymmetry in the chemical potentials) and the magnitude of the coupling. Our numerical runs search for solutions in the density-asymmetry and temperature plane at some fixed value of the coupling constant. The results are shown for a coupling constant parameterized by the (dimensionless) ratio f of the actual coupling parameter to that in the weak-coupling theory, i.e., G . We consider three values of the dimensionless coupling $f = 1.0, 2.0,$ and 2.93 which cover the range from weakly coupled theory ($f = 1$) to the strong coupled theory $f = 2.93$. The latter value is slightly below the zero-temperature critical value of the coupling constant at which the FF phase is extinct.

A. The phase diagram

The phase diagram of the model in the density-asymmetry – temperature plane is shown in Fig. 1 for the (dimensionless) couplings $f = 1.0, 2.0,$ and 2.93 . The lowest value $f = 1$ corresponds to the weak-coupling theory where the occupation numbers of quarks have well defined fermionic nature (occupied states below the Fermi energy and empty states above). For the largest value $f = 2.93$ these features vanish and the occupation numbers are smooth functions of momentum. For obvious reasons, this limit will be referred to as the strong coupling limit. The phase diagram contains three phases: (1) the unpaired state, where the gap Δ and the momentum Q vanish, (2) the BCS state, where $\Delta \neq 0$, but $Q = 0$ and (3) the FF state, where $\Delta \neq 0$ and $Q \neq 0$. These phases meet at a tricritical Lifshitz point (hereafter L point) which divides the critical line of phase transitions to the normal state into two segments. On the small- α segment the normal state transforms to the BCS state, which is uniform in space ($Q = 0$). On the large- α segment the unpaired phase transforms into the superconducting phase with non-uniform order parameter ($Q \neq 0$). The pair-momentum goes to zero as the L point is approached along the critical line. An expansion of the free energy of the system for small order parameter near the L point contains terms $F \sim c_1|\vec{\nabla}\psi|^2 + c_2|\vec{\nabla}^2\psi|^4$. Since on one side of the L point the minimum of the free

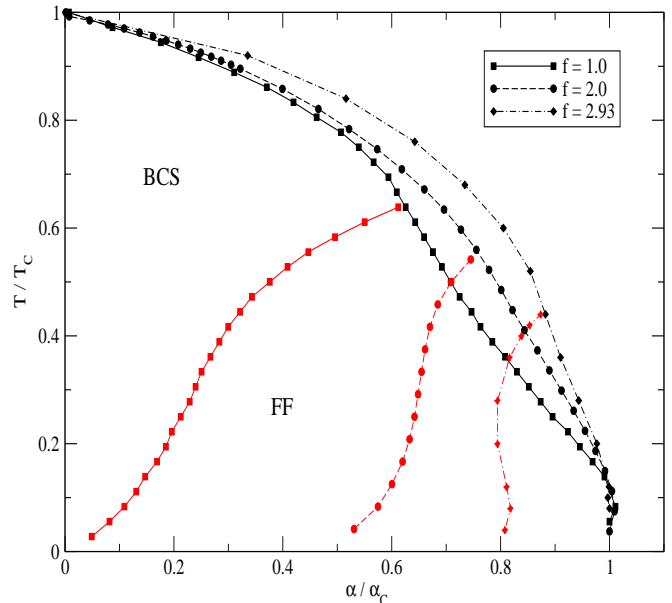


FIG. 1: (Color online) The phase diagram of chiral quark matter for three (dimensionless) couplings $f = 1.0, 2.0$ and 2.93 . For each coupling the x and y axis are normalized to the values of the critical asymmetry $\alpha_c(f)$ at $T = 0$ and the critical temperature $T_c(f)$, respectively. The values of these parameters are: $\alpha_c(1) = 0.18$, $\alpha_c(2) = 0.77$, $\alpha_c(2.93) = 1.0$ and $T_c(1) = 23.0$, $T_c(2) = 144.0$ and $T_c(2.93) = 252.0 \text{ MeV}$. The upper left domains marked as BCS correspond to the BCS state with $Q = 0$. The lower right domains marked as FF correspond to the Fulde-Ferrell state with $Q \neq 0$. The upper right domain corresponds to the unpaired state ($\Delta = 0$). The three phases meet at the (Lifshitz) tricritical point.

energy corresponds to $Q = 0$, while on the other side the minimum corresponds to $Q \neq 0$ the coefficient c_2 must change sign at the L point and c_4 must be positive. This suggests that chiral quark matter belongs to the universality class of paramagnetic-ferromagnetic-helical systems for which these terms lead to the existence of the L point. The critical behavior of the vector Q was determined from renormalization group arguments near the L point [76]. Along the large- α branch the momentum of the condensate varies to leading order as $Q \sim |\bar{\alpha}|^\beta$, where $\beta = 1/2$, $\bar{\alpha} = (\alpha - \alpha_c)/\alpha_c$ and α_c is the critical value of the asymmetry.

The structure of the phase diagram can be understood qualitatively in terms of the quasiparticle spectrum, Eqs. (31) and (32). At nonzero α the Fermi surfaces of the species are mismatched by an amount given by Eq. (32). In the homogeneous BCS state the mismatch is a scalar $\delta\mu$, independent of the direction in momentum space. Because $\cos\theta$ assumes both positive and negative values, the mismatch is “modulated” in momentum space for the FF phase. One can speak of coherence

(or decoherence) to quantify to which extent the Fermi surfaces of the up and down quarks overlap. The coherence is maximal for perfectly overlapping Fermi surfaces ($E_A = 0$). While in the homogeneous phase the coherence decreases as $\delta\mu$ is increased, in the FF phase the decoherence can be compensated as the Fermi surfaces of the majority and minority components come closer together in some directions, which in turn can increase the pairing energy. This, however, increases also the overall kinetic energy of the condensate. The compromise among these two effects can produce an overall gain in the negative condensate energy, which eventually makes the FF phase more favorable than the BCS phase. Nonzero temperature “smears” the Fermi surfaces, i.e., it reduces the mismatch over the range $[\beta E_F(u, d)]^{-1}$, where $E_F(u, d)$ are the Fermi energies of the up and down quarks.

Let us return the phase diagram and comment on its structure. The weakly coupled $T \rightarrow 0$ limit is characterized by the fact that the FF phase is favored at any asymmetry. At $T = 0$ the excitations are confined near the Fermi surface and a small mismatch is sufficient to destroy the BCS state. Nonzero temperatures increase the Fermi surface smearing and the coherence, therefore the domain occupied by the BCS state is larger. Increasing the coupling has two effects: first, the BCS state becomes more robust, as the ratio of the gap $\Delta(T = 0)$ to the average chemical potential $\bar{\mu}$ increases; the occupancy domain of the FF state is correspondingly reduced. Secondly, the nature of the BCS state changes in the sense that the condensate evolves to a state that has characteristics of a homogeneous Bose-Einstein condensate (BEC). The nature of the FF state also changes; in the FF state adjacent to the homogeneous BEC state only the majority distribution has fermionic nature (a pronounced Fermi sphere); the minority component has a shell-structure distribution (for more details see the discussion below). It is evident that there exist a limiting coupling beyond which the FF state is vanishing. We note that a topologically similar phase diagram exists for non-relativistic fermions in weak coupling [77, 78]. Ref. [77] suggests an approximately self-similar evolution of the phase diagram in the strong-coupling regime, which is at variance to the results shown in Fig. 1.

If the transition to the color-superconducting state occurs at sufficiently high densities, newborn compact star will cross the diagram in Fig. 1 starting from the upper left corner and move down the temperatures axis towards nonzero asymmetries. The key implication of the phase diagram is that the asymptotic low-temperature state corresponds to the FF state independent of the magnitude of the flavor asymmetry.

An alternative view on the phase diagram of paired chiral quark matter offers Fig. 2, where the phases are plotted in the temperature and chemical-potential mismatch plane. Consistent with what we have learned from Fig. 1 the domain of occupancy of the FF state shrinks as the coupling is increased, although there is no simple mapping between the two cases. For $f = 1$ and $f = 2$

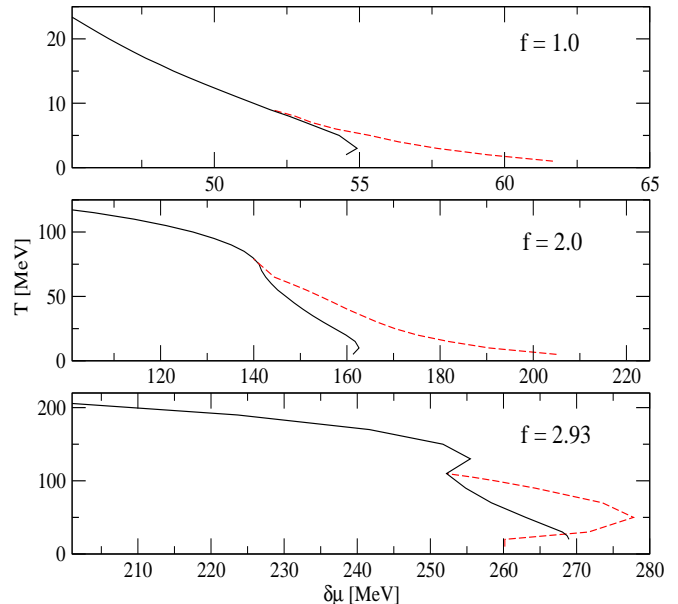


FIG. 2: (Color online) The phase diagram of chiral quark matter in the temperature – chemical potential mismatch ($\delta\mu/2$) plane, for three couplings, $f = 1$ (upper panel), $f = 2$ (middle panel), $f = 2.93$ (lower panel). In each panel the lower left domain corresponds to the BCS state with $Q = 0$, the domain between the solid and the dashed lines, corresponds to the Fulde-Ferrell state with $Q \neq 0$, the remainder domain is occupied by the unpaired state ($\Delta = 0$). The three phases meet at the (Lifshitz) tricritical point.

and for low T the FF state occupies approximately 1/4 of the range of $\delta\mu/2$ values that admit pair correlations; this range is reduced to 0.14 for $f = 2.93$. The zero-temperature gap is $\Delta = 64.7$ MeV in weak coupling; the critical value of the mismatch at which the transition to the BCS takes place is read off to be $\delta\mu_1/\Delta(0) \simeq 0.8$; the transition from the BCS to the FF state takes place at $\delta\mu_2/\Delta(0) \simeq 1$.

B. Temperature-asymmetry dependence of the gap

The detailed features observed in the phase diagram can be understood by examining the behavior of the gap function along vertical cuts of constant asymmetry and horizontal cuts of constant temperature in Fig. 1. We shall first discuss the weak-coupling domain and then simply show that the behavior of the gap function in strong coupling is self-similar to that of weak coupling. Fig. 3 shows the weak-coupling gap as a function of temperature for a range of asymmetries. The curves for non-zero asymmetries can be divided into two segments which are separated by the point where the dotted curves branch off. The high-temperature the segment

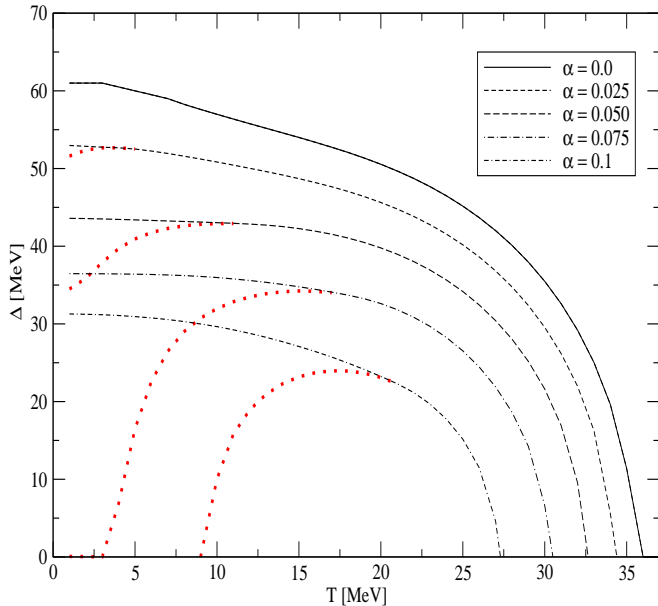


FIG. 3: (Color online) Dependence of the pairing gap for BCS and FF states on temperature for several asymmetries. The FF phase exists in the temperature domain between $T = 0$ and the temperature where the dotted (red online) curves merge with the others. For higher temperatures the superconductor is in the BCS state. The low-temperature behavior of the BCS phase is anomalous as the gap decreases with decreasing temperature and for asymmetries $\alpha \simeq 0.07$ gives rise to a second critical temperature.

corresponds to the BCS state; the temperature dependence of the gap is standard, i.e., $d\Delta(T)/dT < 0$ and the high-temperature asymptotics is $\Delta(\alpha) \sim [T_c(\alpha)(T_c(\alpha) - T)]^{1/2}$, where $T_c(\alpha)$ is the (upper) critical temperature. On the low-temperature segment there are two competing phases (BCS and FF), which have very different temperature dependence of the gap function. The quenching of the BCS gap (dotted lines) as the temperature is decreased is caused by the loss of coherence among the quasiparticles as a consequence of vanishing smearing of the Fermi surfaces with temperature, which scales as $[\beta E_F(u, d)]^{-1}$. Consequently, in the low-temperature segment $d\Delta(T)/dT > 0$ and for large enough asymmetries there exists a lower critical temperature T_c^* [54]. On contrary, for the FF phase $d\Delta(T)/dT < 0$ as is the case in the ordinary (symmetrical) BCS theory. It should be mentioned that the “anomalous” behavior of the BCS gap below the point of bifurcation of the FF state leads to a number of anomalies in the thermodynamic quantities, such as negative superfluid density or negative difference between the normal and superfluid entropies [54]. These anomalies are absent in the FF state [25]. In Fig. 4 we show the gap function along cuts

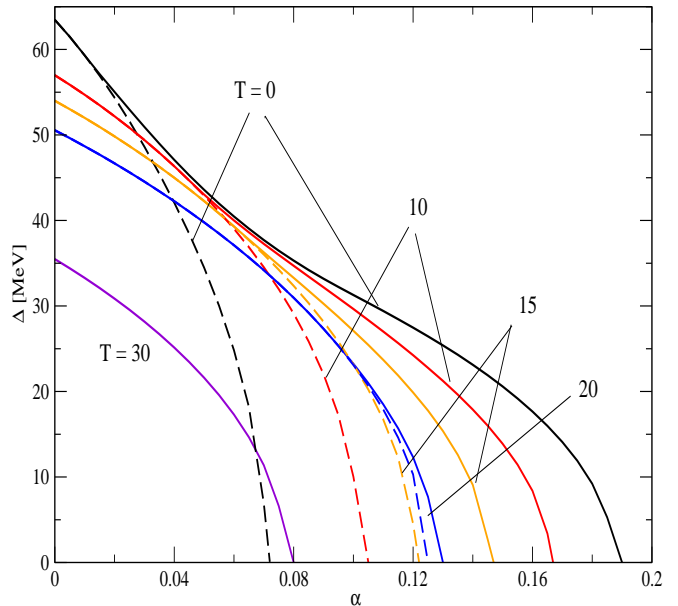


FIG. 4: (Color online) Dependence of the pairing gap for BCS (dashed lines) and FF (solid lines) phases on asymmetry parameter for several temperature labeled in the figure.

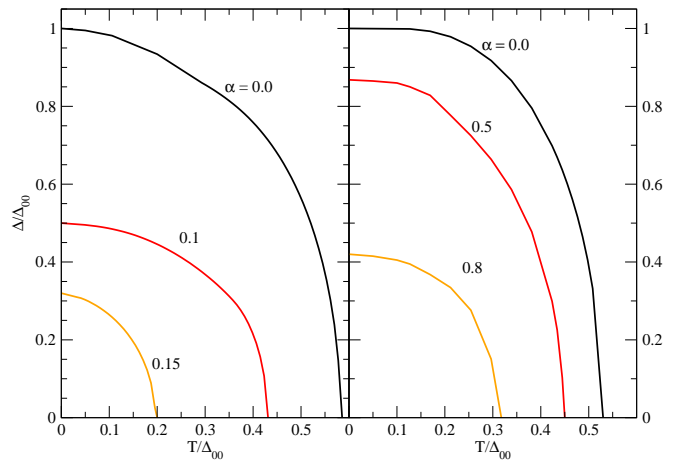


FIG. 5: (Color online) Dependence of the gap function in the the FF (low temperatures) and BCS (high temperatures) phases on temperature for several fixed asymmetries labeled in figure. Left panel corresponds to the weak coupling limit $f = 1$, the right panel to the strong coupling limit $f = 2.93$. The energy scales are given in units of the respective gaps in the zero temperature and symmetric limits Δ_{00} .

of temperature in the phase diagram. As above, there are two segments for each temperature: the low- α do-

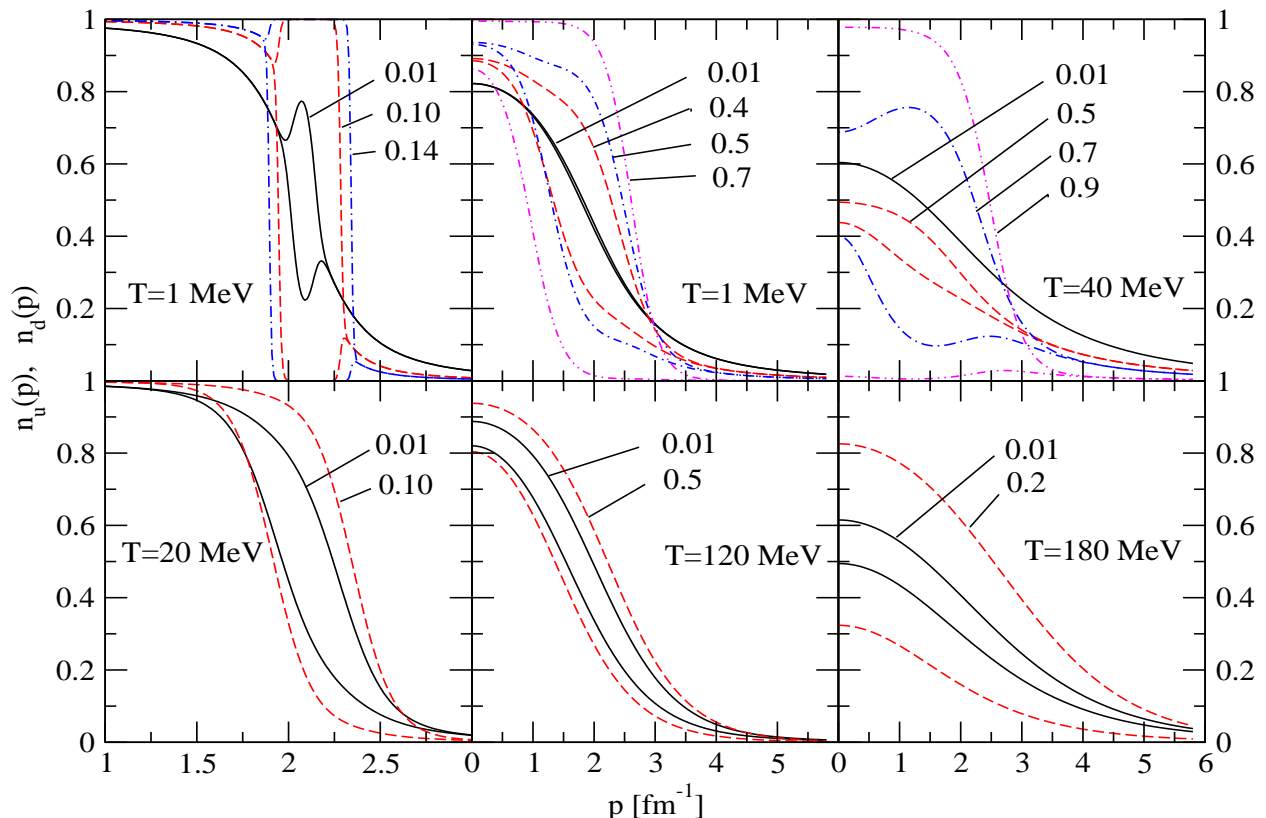


FIG. 6: (Color online) Dependence of occupation numbers on the mode. The majority and minority components are shown for each asymmetry with same style curves. The numeric labels define the density asymmetry parameter α . The left, middle and right panels correspond to the weak $f = 1$, intermediate $f = 2$ and strong $f = 2.93$ coupling limits. The upper row displays the dependence at low temperatures, the lower row – at high temperatures (see the labeling in the figure).

main where only the BCS phase exists and the large- α domain where both BCS (dashed lines) and FF (solid lines) solutions exist, but the FF solution is favored. For small α the gap function is linear in α ; the large- α asymptotics is $\Delta(\alpha) \sim \Delta_{00} (1 - \alpha/\alpha_1)^{1/2}$, where $\alpha_1 \sim \Delta_{00}/\bar{\mu}$ and Δ_{00} is the value of the gap at vanishing temperature and asymmetry. The critical asymmetry α_2 at which the FF phase transforms into the normal phase is a decreasing function of temperature, whereas that for the BCS phase (α_1 above) increases up to the temperature where $\alpha_1 = \alpha_2$; for larger temperature α_1 decreases with temperature. Consequently, in the dominant phase the critical asymmetry always decreases with temperature.

Figure 5 compares the temperature dependence of the gap in the preferred phase (FF phase at low- T , BCS phase at high- T) in the weak-coupling ($f = 1$, left panel) and strong-coupling limits ($f = 2.93$, right panel). We observe that the curves in both limits are self-similar, therefore the qualitative arguments presented for the case of weak coupling should hold also in the case of strong

coupling. The two limits differ, of course, quantitatively, which is manifest in the magnitudes of the asymmetries required to suppress the gap to a given fraction of the gap in the symmetric case.

C. Occupation numbers and wave functions

The integrands of Eqs. (43) and (44) define the occupation numbers $n_{d/u}(p)$ of the down and up quarks (referred also as the majority and the minority components). Their dependence on momentum for a special direction $\cos \theta = 0$ is shown in Fig. 6. The weak-coupling and low-temperature case (left upper panel) develops a “breach” or “blocking region” for large asymmetries, i.e., the minority component is entirely expelled from the blocking region ($n_u = 0$), while the majority component is maximally occupied ($n_d = 1$). In the small α limit occupation numbers are clearly fermionic (with some diffuseness due to the temperature), i.e., the states are filled below a cer-

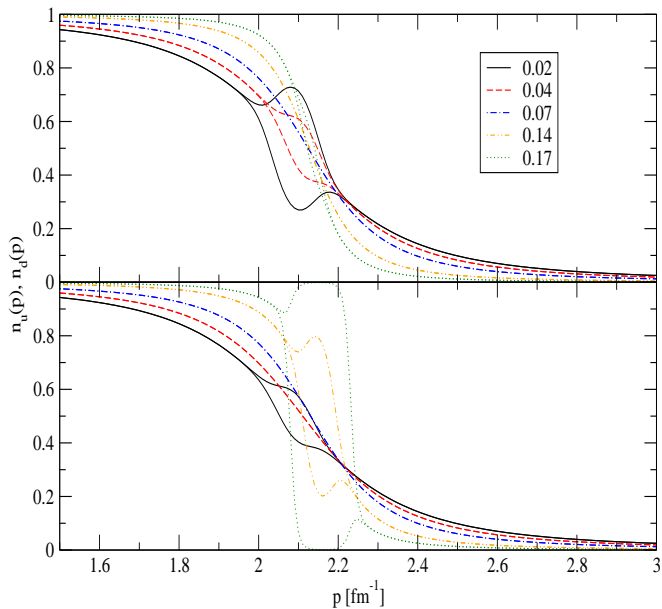


FIG. 7: (Color online) Dependence of occupation numbers on the momentum for weak coupling $f = 1$ and two angles $\theta = 45^\circ$ (upper panel) and $\theta = 90^\circ$ (lower panel). The majority and minority components are shown for each asymmetry with curves of the same style. The numeric labels indicate the density asymmetry parameter α .

tain mode (Fermi momentum) and are empty above. In the high-temperature limit (lower left corner) the breach gets filled in, the occupation numbers are smooth functions of momentum, consequently the high-momentum modes are less populated. In the intermediate-coupling, low-temperature, regime ($f = 2$, middle panel in Fig. 6) the fermionic nature of the occupation numbers is lost, e.g., the zero-momentum modes are not fully populated until large asymmetries are reached. Furthermore, it is not possible to identify a Fermi surface as the modes are populated smoothly (an exception is the population of the majority at near critical asymmetries). Temperature smears out the “knee” in the occupation numbers, as seen in the plot for the intermediate-coupling and high-temperature regime (lower middle panel). The strong-coupling regime $f = 2.93$ can be identified with the Bose-Einstein condensate phase of strongly coupled pairs. At large asymmetries the distribution of the minority component undergoes a topological change, by first developing an empty strip within the distribution function, which is followed at larger asymmetries by a distribution in which modes are populated starting from a certain nonzero value. Thus, the Fermi sphere of the minority component in the BCS limit evolves into a shallow shell structure in the strongly coupled Bose-Einstein condensed limit. Such a behavior has been established both for nonrelativistic [40] and relativistic systems [44] in the

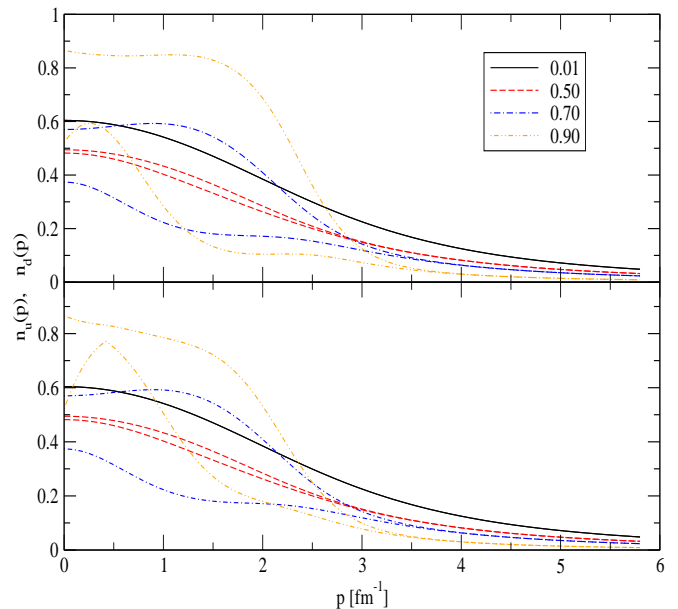


FIG. 8: (Color online) Same as in Fig. 7, but for strong coupling, $f = 2.93$.

case of a homogeneous superconducting phase.

To understand the behavior of the occupation number in the FF phase, we need to look at the cases where $\cos \theta \neq 0$ (the limit $\cos \theta = 0$ discussed above is special as it describes the asymmetric BCS state). Figure 7 shows the occupation numbers in the weak-coupling limit for two fixed angles $\theta = 45^\circ$ (upper panel) and $\theta = 90^\circ$ (lower panel) and for several asymmetries. For fixed angle $\theta = 45^\circ$ increasing the asymmetry has an effect on the occupation number which is opposite to the one observed for $\theta = 0^\circ$ case: for large asymmetries the difference between the occupation numbers disappears, i.e., the superconductor behaves as if it was flavor-symmetric. Thus, asymmetries and angles for which pairing is promoted over the asymmetrical BCS state makes it possible for the FF state to have lower free energy than the BCS state; in effect, the nonzero momentum compensates for the mismatch of the Fermi spheres and restores the coherence needed for pairing to occur. For fixed $\theta = 90^\circ$ the picture is reversed again: increasing the asymmetry a blocking region (breach) develops in the occupation numbers; note however that there is no perfect symmetry in the occupation numbers against rotations by 90° .

Figure 8 shows the same dependence in the case of strong coupling $f = 2.93$. Both for $\theta = 45^\circ$ (upper panel) and for $\theta = 90^\circ$ (lower panel) the occupation numbers move apart with increasing asymmetry, as is the case for $\theta = 0^\circ$. For large asymmetries and nonzero angles the knee in the majority distribution is less pronounced and the minority component does not undergo the topolog-

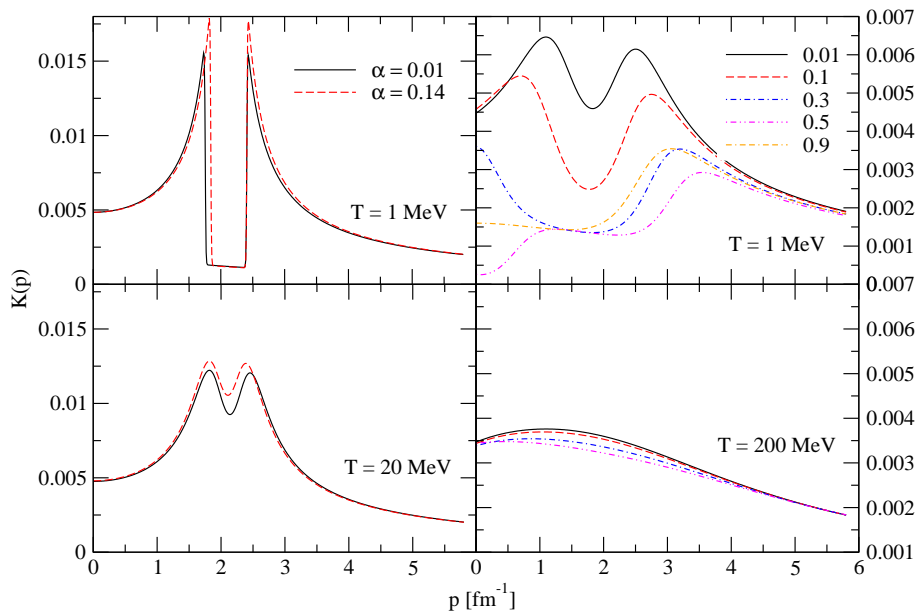


FIG. 9: (Color online) Dependence of the kernel $K(p)$ on the momentum in the two extremes of weak $f = 1$ (left column) and strong couplings $f = 2.93$ (right column). The numeric labels define the density asymmetry parameter α . The upper row corresponds to low temperatures, the lower row – to high temperatures (see the labeling in the figure).

ical change seen for $\theta = 0^\circ$, but the general features of occupation numbers are the same.

Fig. 9 displays the kernel of Eq. (42), which can be written as

$$K(p) = \sum_e \frac{1}{2\sqrt{E_{S,e}^2 + |\Delta^e|^2}} \left\{ \tanh \left[\frac{\beta}{2} E_e^+(\Delta^e) \right] + \tanh \left[\frac{\beta}{2} E_e^-(\Delta^e) \right] \right\}. \quad (50)$$

For contact interactions this kernel is the product of the imaginary part of the (on-shell) retarded propagator and the Pauli operator (the sum of tanh terms). Physically, it has been interpreted as the wave function of the Cooper pairs, since in the non-relativistic limit it obeys a Schrödinger-type eigenvalue equation. The prefactor of the Pauli operator is a smooth function of momentum with a maximum at the Fermi surface, where $E_{S,e} = 0$.

The modes that essentially contribute to the pairing correlations in different regimes can be identified from Fig. 9. In the low-temperature regime $K(p)$ has two maxima which are separated by a depression around the Fermi momentum. This behavior is the consequence of the blocking region in the occupation number discussed above. To see this we note that the Pauli operator (up to an irrelevant constant) can be rewritten as $1 - f_u(p) - f_d(p)$, where $f_{u/d}(p)$ are the u and d quark distributions. We have seen that in the blocking region $f_d(p) \rightarrow 1$ and $f_u(p) \rightarrow 0$, as a consequence the function $K(p)$ is depressed for modes within the blocking region. Increasing the temperature smears out the structures seen in the low-temperature case, in agree-

ment with the smearing seen in the occupation numbers. In the strong-coupling and low-temperature limit (left upper panel) the double-structure is broadened due to the correlations rather than the temperature. For large asymmetries there is a topological change in the structure of the Fermi sphere of the minority which is seen to depress the low-momentum structure from the minority component, i.e., the contribution to the pairing comes only from the vicinity of the Fermi sphere of the majority component.

The quantity $K(p)$ can be interpreted as a wave function of the Cooper pairs. It is seen that in the weak-coupling limit it is well localized in momentum space, i.e., the Cooper pairs have structure which is broad in real space (large coherence length). The picture is reversed in the strong coupling limit, where $K(p)$ is a broad function of momentum, therefore it is well localized in the real space, i.e., it corresponds to strongly bound Bose molecules. The temperature suppression of the pairing correlation in either limit can be seen by comparing the upper and lower panels of Fig. 9.

We consider next the Fourier transform of kernel $K(p)$ to understand the spatial structure of the Cooper pairs. The Fourier image of $K(p)$ function has the physical interpretation of the Cooper pair “wave-function”, which we define as

$$\begin{aligned} \psi(\mathbf{r}) &= \sqrt{N} \int \frac{d^3p}{(2\pi)^3} [K(p, \Delta) - K(p, 0)] e^{i\mathbf{p}\cdot\mathbf{r}} \\ &= \frac{\sqrt{N}}{2\pi r^2} \int_0^\infty dp p [K(p, \Delta) - K(p, 0)] \sin(pr), \end{aligned} \quad (51)$$

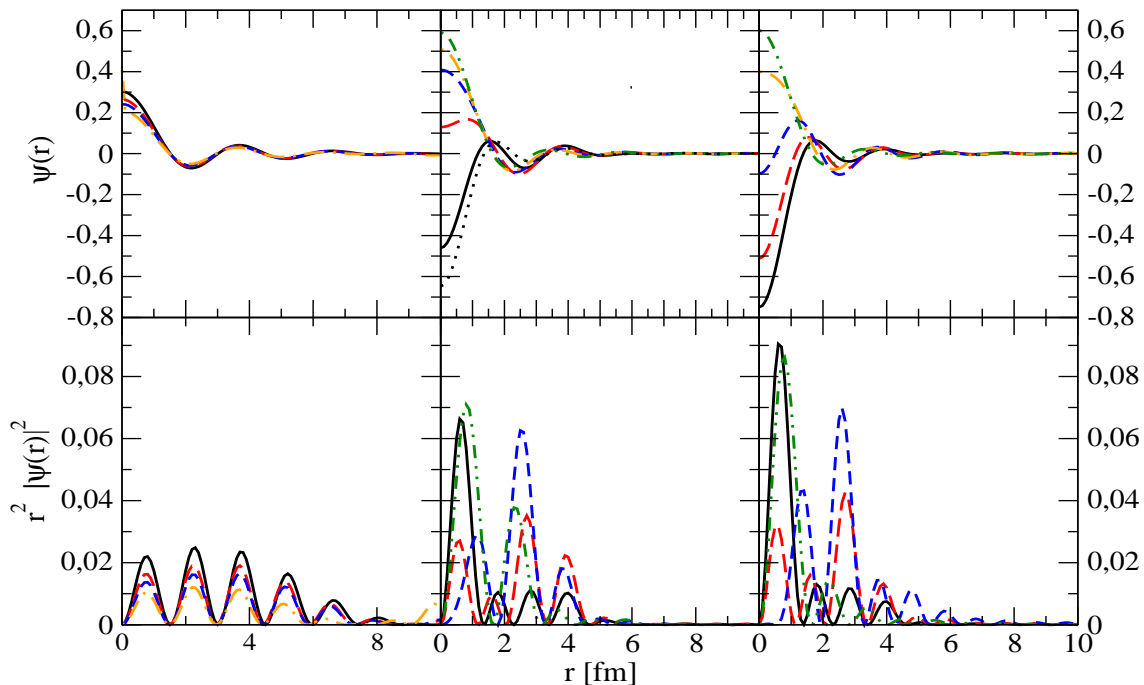


FIG. 10: (Color online) *Upper panel:* The wave-function of Cooper pairs for weak $f = 1$ (left column), intermediate $f = 2$ (middle column) and strong $f = 2.93$ (right column) coupling. The asymmetries are $\alpha = 0.1$ (solid line, black online), 0.2 (dashed line, red online), 0.3 (short-dashed line, blue online), 0.4 (dashed-double-dotted line, orange online), and 0.5 (dashed-double-dotted line, green online). The dotted curve shows the results for $\alpha = 0.01$ at intermediate coupling; in the case of weak coupling the $\alpha = 0.01$ curve coincides with $\alpha = 0.1$ one. The temperature is $T = 1$ MeV in the left panel, and $T = 40$ MeV in the middle and right panels.

where N is a constant that is determined from the normalization condition

$$N \int d^3r |\psi(\mathbf{r})|^2 = 1. \quad (52)$$

In Eq. (51) we subtracted from the kernel its value in the normal state $K(p, 0)$ to regularize the integral, which is otherwise divergent. Cut-off regularization of this strongly oscillating integral is not appropriate. The mean-square radius of a Cooper pair is defined via the second-moment integral of the density probability

$$\langle r^2 \rangle = \int d^3r r^2 |\psi(\mathbf{r})|^2. \quad (53)$$

The coherence length, i.e., the spatial extension of a Cooper pair, is defined as $\xi = \sqrt{\langle r^2 \rangle}$. The regimes of strong and weak coupling can be identified by comparing the coherence length to the mean interparticle distance, which is defined as $d = [3/4\pi(n_u + n_b)]^{1/3}$. We obtain $d = 0.6$ fm, for $n_B = 0.55$ fm $^{-3}$, and $\xi(f = 1) = 5.416942$, $\xi(f = 2) = 1.9$, and $\xi(f = 2.93) = 1.9$.

Fig. 10, upper panel, shows the wave-function of Cooper pairs as a function of radial distance for various coupling constants. In weak coupling, the wave function has well-defined oscillatory form which extends over many periods of the interparticle distance. Such a state corresponds to the BCS theory where the spatial correlations are characterized by scales that are much larger than the interparticle distance. For intermediate and strong coupling the wave function is increasingly concentrated at the origin with few periods of oscillations at most. The strong-coupling limit corresponds to pairs that are well localized in space within a small radius. This regime has clearly BEC character, where the pair-correlations extend over distances comparable to the interparticle distance. It is seen that in weak coupling the wave function is almost independent of the asymmetry, whereas in strong coupling this dependence is substantial. The complementary lower panel of Fig. 10 shows the quantity $r^2|\psi(\mathbf{r})|^2$. In strong coupling the spatial correlation is dominated by a single peak, which indicates a tightly bound state close to the origin. The existence of residual oscillations indicates that there is no

unique bound state formed at such coupling, but the tendency towards its formation is clearly seen. An oscillatory structure appears in the intermediate-coupling regime indicating a transition from the BEC to the BCS regime. In the weak-coupling limit the short-range correlations disappear leaving behind a BCS state that is correlated over large distances. At low and high asymmetries the strong-coupling peaks are well defined, whereas at intermediate asymmetries the weight of the function is distributed among several peaks.

IV. CONCLUSIONS AND OUTLOOK

We have calculated the phase diagram of chiral quark matter in the temperature-flavor asymmetry plane, in the case where there are three competing phases - the homogeneous BCS state, the inhomogeneous FF state and unpaired quark matter. The theory is formulated in the chiral limit of massless up and down quarks interacting with a contact interaction obtained from integrating out the gluonic degrees of freedom. Fluctuations beyond mean-field have not been included. We have studied how the structure of the phase diagram changes as the attractive coupling strength is increased. At weak coupling and zero temperature the FF state is favored for arbitrary asymmetries. At higher temperatures its domain of occupancy is restricted to increasingly larger asymmetries. The phase diagram features a tricritical Lifshitz point, where the BCS, FF and normal states meet. Near this point our system belongs to the universality class of paramagnetic-ferromagnetic-helical systems, for which the critical exponents near the Lifshitz point are known. In particular, the momentum scale characterizing the breaking of translational invariance has a critical exponent of $1/2$ to leading order. As the coupling is increased the domain occupied by the BCS phase relative to the FF phase increases. There exists a critical coupling at which the FF phase disappears entirely. This transformation with coupling shifts the tri-critical point to larger asymmetries, where it disappears when the FF state is extinct. The strong-coupling limit of the FF state is particularly interesting, since at such coupling the system enters the BEC regime, as is evidenced by the momentum dependence of the occupation numbers and the ratio of the coherence length to the interparticle distance being of the order of unity. This new regime can be identified with a current-carrying Bose-Einstein condensate of bound chiral up and down quarks.

The analysis of the dependence of the gap function as a function of temperature and asymmetry shows that this functional dependence carries over to the intermediate- and strong-coupling regimes in a self-similar manner. In particular, the temperature dependence of the gap in the BCS and FF states does not show anomalies present in the asymmetric BCS state, i.e., their behavior is self-similar to the one observed in flavor-symmetric BCS phase. Our analysis of the momentum dependence of

the occupation numbers shows that in the BCS state, and in the FF at special angle for which the condensate momentum $Q = 0$, the minority component contains a blocking region (breach) around the Fermi sphere in the weak-coupling limit, which engulfs more low-momentum modes as the coupling increases, and eventually leads to a topological change in strong coupling, where the minority Fermi sphere contains either two occupied strips or an empty sphere [40, 44]. We show that at arbitrary angles, i.e., for (effectively) non-zero Q , the blocking region is filled in and the momentum dependence of the occupation numbers is smooth; this anti-blocking effect is a direct consequence of the mechanism of restoration of the pair correlation in the FF state due to non-zero Q . This mechanism can be seen in the momentum dependence of the Cooper pair wave function. In the asymmetric BCS state the blocking of minority occupation numbers leads to a depletion of in the wave-function, and hence reduction of the gap. The anti-blocking effect in the occupation numbers of the FF phase, inverts this tendency by restoring the wave-function, and therefore pair correlations. In weak coupling the momentum dependence of the occupation numbers is a Fermi distribution (neglecting for the sake of argument the changes near the Fermi surface due to pairing and flavor asymmetry). In strong coupling, the momentum dependence does not show a step-function behavior, rather one deals with a broad distribution with modes occupied far away from the actual Fermi sphere. This form of occupation numbers suggest that we work effectively in the Bose-Einstein-condensed limit. This is further confirmed by our study of the spatial structure of the Cooper wave function. In the weak-coupling limit it describes a macroscopically coherent state characterized by wave function oscillations that extend over distances which are much larger than the interparticle distance. In the strong-coupling limit the nodal structure of the wave function disappears; instead one observes a well developed single structure, which is interpreted as a bound state of up and down quarks (and anti-quarks) forming a boson. This picture lends support to the claim that in strong coupling we observe a new regime of the FF state which corresponds to the current-carrying Bose condensate.

Minimal extensions of the present model to account for electric and color charge neutralities and β -equilibrium among quarks will make it suitable for applications to compact star physics [25, 79, 80, 81].

The strong-coupling limit of the FF phase is not likely to be realized in quark matter in compact stars. Currently accepted parameters predict quark superconductivity well in the BCS regime. Nevertheless, our study of the strong-coupling limit, and identification of a new regime of current-carrying Bose condensate, may not be entirely of academic interest. Cold fermionic atoms offer an excellent laboratory where the properties of the phases of imbalanced fermions are being tested. The diversity of such systems and the methods (ranging, e.g., from direct imaging of the atomic clouds to studying the vortex lat-

tices) hold the promise that our findings could be tested in experiments [49, 50, 51, 52, 53, 54, 55, 56, 57, 58]. The relativistic (chiral) aspects of our study could be relevant for the studies of graphene - another condensed matter system, where electrons are described by the Dirac equation and, therefore, exhibit relativistic dynamics [59, 60, 61, 62].

was, in part, supported by the Deutsche Forschungsgemeinschaft (Grant SE 1836/1-1) and the Extreme Matter Institute (EMMI).

Acknowledgments

We are grateful to M. Alford, M. Buballa, X. Huang, M. Kuclic, and H. Warringa for discussions. This work

APPENDIX A: THE QUASIPARTICLE SPECTRUM

In this appendix we calculate the explicit form of the quasiparticle spectrum in the FF state from Eq. (29)

$$\left(\tilde{G}_{0i}^{-f}\right)^{-1} \left(\tilde{G}_{0j}^{+g}\right)^{-1} - \sum_e |\Delta^{efg}|^2 \Lambda^e(\mathbf{k}), = 0, \quad (\text{A1})$$

where the Green's functions in the chiral limit are given by

$$[\tilde{G}_{0i}^{\pm f}]^{-1} = \gamma^\mu \left(\pm \frac{Q_\mu}{2} + k_\mu \right) \pm \mu_i^f \gamma_0. \quad (\text{A2})$$

The explicit form of Eq. (A1) is

$$\left[\gamma^\mu \left(-\frac{Q_\mu}{2} + k_\mu \right) - \mu_i^f \gamma_0 \right] \left[\gamma^\mu \left(\frac{Q_\mu}{2} + k_\mu \right) + \mu_j^g \gamma_0 \right] - \sum_e |\Delta^{efg}|^2 \Lambda^e(\mathbf{k}) = 0. \quad (\text{A3})$$

Upon multiplying this equation from left and right by γ^0 one finds

$$\left[\gamma^0 \gamma^\mu \left(-\frac{Q_\mu}{2} + k_\mu \right) - \mu_i^f \right] \left[\gamma^\mu \gamma^0 \left(\frac{Q_\mu}{2} + k_\mu \right) + \mu_j^g \right] - \sum_e |\Delta^{efg}|^2 \gamma^0 \Lambda^e(\mathbf{k}) \gamma^0 = 0 \quad (\text{A4})$$

We further separate the time and space components and use the projectors to positive and negative energy states $\Lambda^\pm(\mathbf{k}) = (1 + \boldsymbol{\alpha} \cdot \mathbf{k}/|\mathbf{k}|)/2$ and their property

$$|\mathbf{k}|[\Lambda^+(\mathbf{k}) - \Lambda^-(\mathbf{k})] = \boldsymbol{\alpha} \cdot \mathbf{k}, \quad (\text{A5})$$

to eliminate the quantity $\boldsymbol{\alpha} = \gamma^0 \boldsymbol{\gamma}$. Since the dispersion relations for the particles and anti-particles separate, we shall keep only the particle states below to obtain

$$\left[-\frac{1}{2} \Lambda^+(\hat{\mathbf{k}} \cdot \mathbf{Q}) + \Lambda^+|\mathbf{k}| + k_0 - \mu_i^f \right] \left[-\frac{1}{2} \Lambda^+(\hat{\mathbf{k}} \cdot \mathbf{Q}) - \Lambda^+|\mathbf{k}| + k_0 + \mu_j^g \right] - |\Delta^{fg}|^2 \Lambda^+(\mathbf{k}) = 0. \quad (\text{A6})$$

The averaged and mismatched chemical potentials are defined as

$$\bar{\mu} = \frac{1}{2}(\mu_i^f + \mu_j^g), \quad \delta\mu = \frac{1}{2}(\mu_i^f - \mu_j^g), \quad (\text{A7})$$

i.e., $\mu_i^f = \bar{\mu} + \delta\mu$ and $\mu_j^g = \bar{\mu} - \delta\mu$. Substituting these relations we obtain

$$\left[-\frac{1}{2} \Lambda^+(\hat{\mathbf{k}} \cdot \mathbf{Q}) + \Lambda^+|\mathbf{k}| + k_0 - \bar{\mu} - \delta\mu \right] \left[-\frac{1}{2} \Lambda^+(\hat{\mathbf{k}} \cdot \mathbf{Q}) - \Lambda^+|\mathbf{k}| + k_0 + \bar{\mu} - \delta\mu \right] - |\Delta^{fg}|^2 \Lambda^+(\mathbf{k}) = 0. \quad (\text{A8})$$

The terms that do not contain the positive projector can be multiplied by $\Lambda^+ + \Lambda^- = 1$, i.e. they equally contribute to the dispersions of the positive and negative energy state particles. We obtain

$$\left[k_0 - \frac{1}{2}(\hat{\mathbf{k}} \cdot \mathbf{Q}) - \delta\mu + |\mathbf{k}| - \bar{\mu} \right] \left[k_0 - \frac{1}{2}(\hat{\mathbf{k}} \cdot \mathbf{Q}) - \delta\mu - (|\mathbf{k}| - \bar{\mu}) \right] - |\Delta_{ij}^{fg}|^2 = 0, \quad (\text{A9})$$

or

$$\left[k_0 - \frac{1}{2}(\hat{\mathbf{k}} \cdot \mathbf{Q}) - \delta\mu \right]^2 - (|\mathbf{k}| - \bar{\mu})^2 - |\Delta_{ij}^{fg}|^2 = 0. \quad (\text{A10})$$

The dispersion relation is the solution of Eq. (A10)

$$k_0 = \frac{1}{2}(\hat{\mathbf{k}} \cdot \mathbf{Q}) + \delta\mu \pm \sqrt{(|\mathbf{k}| - \bar{\mu})^2 + |\Delta_{ij}^{fg}|^2}. \quad (\text{A11})$$

-
- [1] D. Bailin and A. Love, Phys. Rept. **107**, 325 (1984).
[2] K. Rajagopal and F. Wilczek, arXiv:hep-ph/0011333; M. G. Alford, Ann. Rev. Nucl. Part. Sci. **51**, 131 (2001) [arXiv:hep-ph/0102047]; S. Reddy, Acta Phys. Polon. B **33**, 4101 (2002) [arXiv:nucl-th/0211045]; D. H. Rischke, Prog. Part. Nucl. Phys. **52**, 197 (2004) [arXiv:nucl-th/0305030]; I. A. Shovkovy, Found. Phys. **35**, 1309 (2005) [arXiv:nucl-th/0410091]; M. Huang, Int. J. Mod. Phys. E **14**, 675 (2005) [arXiv:hep-ph/0409167]; M. Buballa, Phys. Rep. **407**, 205 (2005); M. Alford and K. Rajagopal, in *Pairing in Fermionic Systems*, edited by A. Sedrakian, J. W. Clark and M. Alford, (World Scientific, Singapore, 2006), p. 1, arXiv:hep-ph/0606157; T. Schafer, *ibid.*, p. 109, arXiv:nucl-th/0602067; D. K. Hong, arXiv:0903.2322 [hep-ph]. M. G. Alford, A. Schmitt, K. Rajagopal and T. Schafer, Rev. Mod. Phys. **80**, 1455 (2008) [arXiv:0709.4635 [hep-ph]].
[3] M. Baldo, M. Buballa, F. Burgio, F. Neumann, M. Oertel and H. J. Schulze, Phys. Lett. B **562**, 153 (2003) [arXiv:nucl-th/0212096].
[4] M. Buballa, F. Neumann, M. Oertel and I. Shovkovy, Phys. Lett. B **595**, 36 (2004) [arXiv:nucl-th/0312078].
[5] H. Grigorian, D. Blaschke and D. N. Aguilera, Phys. Rev. C **69**, 065802 (2004) [arXiv:astro-ph/0303518].
[6] S. B. Ruester and D. H. Rischke, Phys. Rev. D **69**, 045011 (2004) [arXiv:nucl-th/0309022].
[7] M. Alford and S. Reddy, Astrophys. J. **629**, 969 (2005) [arXiv:nucl-th/0411016].
[8] C. Q. Ma and C. Y. Gao, Eur. Phys. J. A **34**, 153 (2007) [arXiv:0706.3243 [astro-ph]].
[9] N. Ippolito, M. Ruggieri, D. Rischke, A. Sedrakian and F. Weber, Phys. Rev. D **77**, 023004 (2008) [arXiv:0710.3874 [astro-ph]].
[10] G. Pagliara and J. Schaffner-Bielich, Phys. Rev. D **77**, 063004 (2008) [arXiv:0711.1119 [astro-ph]].
[11] D. B. Blaschke, D. Gomez Dumm, A. G. Grunfeld, T. Klahn and N. N. Scoccola, Phys. Rev. C **75**, 065804 (2007) [arXiv:nucl-th/0703088].
[12] C. Schaab, D. Voskresensky, A. D. Sedrakian, F. Weber and M. K. Weigel, Astron. Astrophys. **321**, 591 (1997) [arXiv:astro-ph/9605188].
[13] H. Grigorian, D. Blaschke and D. Voskresensky, Phys. Rev. C **71**, 045801 (2005) [arXiv:astro-ph/0411619].
[14] D. Page, J. M. Lattimer, M. Prakash and A. W. Steiner, Astrophys. J. Suppl. **155**, 623 (2004) [arXiv:astro-ph/0403657].
[15] D. Page, U. Geppert and F. Weber, Nucl. Phys. A **777**, 497 (2006) [arXiv:astro-ph/0508056].
[16] A. Sedrakian, Prog. Part. Nucl. Phys. **58**, 168 (2007) [arXiv:nucl-th/0601086].
[17] P. Fulde and R. A. Ferrell, Phys. Rev. **135**, A550 (1964).
[18] A. I. Larkin and Yu. N. Ovchinnikov, Zh. Eksp. Teor. Fiz. **47**, 1136 (1964) [Sov. Phys. JETP **20**, 762 (1965)].
[19] S. Takada and T. Izuyama, Prog. Theor. Phys. **41**, 635 (1969).
[20] M. G. Alford, J. A. Bowers and K. Rajagopal, Phys. Rev. D **63**, 074016 (2001) [arXiv:hep-ph/0008208].
[21] I. Giannakis and H. C. Ren, Phys. Lett. B **611**, 137 (2005) [arXiv:hep-ph/0412015].
[22] T. Schafer, Phys. Rev. Lett. **96**, 012305 (2006) [arXiv:hep-ph/0508190].
[23] K. Fukushima, Phys. Rev. D **73**, 094016 (2006) [arXiv:hep-ph/0603216].
[24] O. Kiriyama, D. H. Rischke and I. A. Shovkovy, Phys. Lett. B **643**, 331 (2006) [arXiv:hep-ph/0606030].
[25] L. He, M. Jin and P. Zhuang, Phys. Rev. D **75**, 036003 (2007) [arXiv:hep-ph/0610121].
[26] J. A. Bowers and K. Rajagopal, Phys. Rev. D **66**, 065002 (2002) [arXiv:hep-ph/0204079].
[27] R. Casalbuoni, R. Gatto, N. Ippolito, G. Nardulli and M. Ruggieri, Phys. Lett. B **627**, 89 (2005) [arXiv:hep-ph/0507247].
[28] K. Rajagopal and R. Sharma, Phys. Rev. D **74**, 094019 (2006) [arXiv:hep-ph/0605316].
[29] K. Rajagopal and R. Sharma, J. Phys. G **32**, S483 (2006) [arXiv:hep-ph/0606066].
[30] M. Mannarelli, K. Rajagopal and R. Sharma, Phys. Rev. D **73**, 114012 (2006) [arXiv:hep-ph/0603076].
[31] N. D. Ippolito, G. Nardulli and M. Ruggieri, JHEP **0704**, 036 (2007) [arXiv:hep-ph/0701113].
[32] E. V. Gorbar, M. Hashimoto and V. A. Miransky, Phys.

- Lett. B **632**, 305 (2006) [arXiv:hep-ph/0507303].
- [33] E. V. Gorbar, M. Hashimoto and V. A. Miransky, Phys. Rev. D **75**, 085012 (2007) [arXiv:hep-ph/0701211].
- [34] A. Gerhold, T. Schafer and A. Kryjevski, Phys. Rev. D **75**, 054012 (2007) [arXiv:hep-ph/0612181].
- [35] H. Mütter and A. Sedrakian, Phys. Rev. Lett. **88**, 252503 (2002) [arXiv:cond-mat/0202409].
- [36] H. Mütter and A. Sedrakian, Phys. Rev. C **67**, 015802 (2003) [arXiv:nucl-th/0209061]; H. Mütter and A. Sedrakian, Phys. Rev. D **67**, 085024 (2003) [arXiv:hep-ph/0212317].
- [37] A. Sedrakian, in *Superdense QCD Matter and Compact Stars*, edited by D. Blaschke and D. Sedrakian, (Springer, Dordrecht, 2006), p. 209, arXiv:nucl-th/0312053.
- [38] A. Sedrakian and J. W. Clark, in *Pairing in Fermionic Systems*, edited by A. Sedrakian, J. W. Clark and M. Alford, (World Scientific, Singapore, 2006), p. 135, arXiv:nucl-th/0607028; A. Sedrakian and J. W. Clark, in *Recent Progress in Many-Body Theories 14*, edited by G. E. Astrakharchik, J. Boronat, and F. Mazzanti, (World Scientific, Singapore, 2007) pg. 138. arXiv:0710.0779 [nucl-th].
- [39] P. Nozieres and S. Schmitt-Rink, J. Low. Temp. Phys. **59**, 195 (1985).
- [40] U. Lombardo, P. Nozieres, P. Schuck, H. J. Schulze and A. Sedrakian, Phys. Rev. C **64**, 064314 (2001) [arXiv:nucl-th/0109024].
- [41] H. Abuki, Nucl. Phys. A **791**, 117 (2007) [arXiv:hep-ph/0605081].
- [42] E. Gubankova, A. Schmitt and F. Wilczek, Phys. Rev. B **74**, 064505 (2006) [arXiv:cond-mat/0603603].
- [43] B. Chatterjee, H. Mishra and A. Mishra, Phys. Rev. D **79**, 014003 (2009) [arXiv:0804.1051 [hep-ph]].
- [44] J. Deng, J. c. Wang and Q. Wang, Phys. Rev. D **78**, 034014 (2008) [arXiv:0803.4360 [hep-ph]].
- [45] M. Kitazawa, D. H. Rischke and I. A. Shovkovy, Prog. Theor. Phys. Suppl. **168**, 389 (2007) [arXiv:0707.3966 [nucl-th]].
- [46] L. He and P. Zhuang, Phys. Rev. D **76**, 056003 (2007) [arXiv:0705.1634 [hep-ph]].
- [47] G. f. Sun, L. He and P. Zhuang, Phys. Rev. D **75**, 096004 (2007) [arXiv:hep-ph/0703159].
- [48] J. Deng, A. Schmitt and Q. Wang, Phys. Rev. D **76**, 034013 (2007) [arXiv:nucl-th/0611097].
- [49] G. B. Partridge, W. Li, Y. A. Liao, R. G. Hulet, M. Haque and H. T. C. Stoof, Phys. Rev. Lett. **97**, 190407 (2006) [arXiv:cond-mat/0608455].
- [50] R. Sharma and S. Reddy, Phys. Rev. A **78**, 063609 (2008) [arXiv:0804.2280 [cond-mat.supr-con]].
- [51] S. Giorgini, L. P. Pitaevskii and S. Stringari, Rev. Mod. Phys. **80**, 1215 (2008).
- [52] D. E. Sheehy and L. Radzihovsky, Annals Phys. **322**, 1790 (2007).
- [53] L. y. He, M. Jin and P. f. Zhuang, Phys. Rev. B **74**, 214516 (2006) [arXiv:cond-mat/0606322].
- [54] A. Sedrakian and U. Lombardo, Phys. Rev. Lett. **84**, 602 (2000); A. Sedrakian, H. Mütter and A. Polls, Phys. Rev. Lett. **97**, 140404 (2006) [arXiv:cond-mat/0605085].
- [55] L. He, M. Jin and P. f. Zhuang, Phys. Rev. B **73**, 214527 (2006) [arXiv:cond-mat/0601147].
- [56] K. Yang, in *Pairing in Fermionic Systems*, edited by A. Sedrakian, J. W. Clark and M. Alford, (World Scientific, Singapore, 2006), p. 253, arXiv:cond-mat/0603190; H. Caldas, *ibid.*, p. 269, arXiv:cond-mat/0605005.
- [57] A. Sedrakian, J. Mur-Petit, A. Polls and H. Mütter, Phys. Rev. A **72**, 013613 (2005) [arXiv:cond-mat/0504511].
- [58] D. T. Son and M. A. Stephanov, Phys. Rev. A **74**, 013614 (2006) arXiv:cond-mat/0507586.
- [59] M. Creutz, JHEP **0804**, 017 (2008) [arXiv:0712.1201 [hep-lat]].
- [60] B. Uchoa and A. H. Castro Neto, Phys. Rev. Lett. **98**, 146801 (2007).
- [61] N. B. Kopnin and E. B. Sonin, Phys. Rev. Lett. **100**, 246808 (2008)
- [62] E. V. Gorbar, V. P. Gusynin, V. A. Miransky and I. A. Shovkovy, Phys. Rev. B **78**, 085437 (2008) [arXiv:0806.0846 [cond-mat.mes-hall]].
- [63] N. Iwamoto, Phys. Rev. Lett. **44**, 1637 (1980).
- [64] M. Alford, P. Jotwani, C. Kouvaris, J. Kundu and K. Rajagopal, Phys. Rev. D **71**, 114011 (2005) [arXiv:astro-ph/0411560].
- [65] P. Jaikumar, C. D. Roberts and A. Sedrakian, Phys. Rev. C **73**, 042801 (2006) [arXiv:nucl-th/0509093].
- [66] R. Anglani, G. Nardulli, M. Ruggieri and M. Mannarelli, Phys. Rev. D **74**, 074005 (2006) [arXiv:hep-ph/0607341].
- [67] S. Popov, H. Grigorian and D. Blaschke, Phys. Rev. C **74**, 025803 (2006) [arXiv:nucl-th/0512098].
- [68] D. Blaschke and H. Grigorian, Prog. Part. Nucl. Phys. **59**, 139 (2007) [arXiv:astro-ph/0612092].
- [69] M. Mannarelli, K. Rajagopal and R. Sharma, Prog. Theor. Phys. Suppl. **174**, 39 (2008).
- [70] L.-M. Lin, Phys. Rev. D **76**, 081502(R) (2007).
- [71] B. Haskell, N. Andersson, D. I. Jones, and L. Samuelsson, Phys. Rev. Lett. **99**, 231101 (2007).
- [72] B. Knippel and A. Sedrakian, Phys. Rev. D **79**, 083007 (2009). arXiv:0901.4637 [astro-ph.SR].
- [73] B. Abbott, *et al.* (LIGO Scientific Collaboration) Astrophys. J. Letters **683**, 45 (2008).
- [74] We assume that there are no external fields, so that the expectation value of the gluon field $\langle A_\mu^a(x) \rangle$ vanishes.
- [75] S. B. Rüster, V. Werth, M. Buballa, I. A. Shovkovy and D. H. Rischke, Phys. Rev. D **72**, 034004 (2005) [arXiv:hep-ph/0503184].
- [76] R. M. Hornreich, M. Luban and S. Shtrikman, Phys. Rev. Lett. **35** 1678 (1975).
- [77] T. Mizushima, K. Machida and M. Ichioka, Phys. Rev. Lett. **94**, 060404 (2005).
- [78] S. Mao, X. Huang and P.-f. Zhuang, Phys. Rev. C **79**, 034304 (2009).
- [79] D. D. Dietrich and D. H. Rischke, Prog. Part. Nucl. Phys. **53**, 305 (2004) [arXiv:nucl-th/0312044].
- [80] H. J. Warringa, arXiv:hep-ph/0606063.
- [81] I. Giannakis, D. f. Hou and H. C. Ren, Phys. Lett. B **631**, 16 (2005) [arXiv:hep-ph/0507306].